VACUUM INSULATION

Being devoid of free charge carriers, a vacuum, in principle, is an ideal electrical insulating medium. Hence, if a potential difference is applied between a pair of conducting electrodes, separated by a spacing d in a vacuum, the resulting vacuum gap should be able to support very high voltages or electric fields. In principle, for devices that operate in a vacuum such as electron beam guns, X-ray generators, microwave tubes, and particle beam accelerators, the vacuum medium should act as an ideal insulator, supporting extremely high voltages without loss of insulation. However, in practice, when the applied field exceeds a threshold value, the vacuum gap fails by the formation of an electrical discharge or arc that short circuits (breaks down) the vacuum space between the electrodes. Hence, there are at least three main issues: (1) From a theoretical point of view, what are the factors that contribute to a vacuum breakdown and by what mechanisms? (2) From a practical point of view, how can we put the maximum voltage across a vacuum gap (VG) of given dimensions? (3) Are there ways to harness the vacuum discharge for practical applications? We shall address each of the above issues.

VACUUM GAP BREAKDOWN

For vacuum gaps of finite dimensions (< tens of centimeters), the electrodes (anode and cathode) are the main sources of charge carriers. Hence, breakdown processes must be based on emission of charged particles, gas desorption, or an increase in the local metal vapor pressure, all associated with the electrodes.

The early studies of VG high voltage phenomena was conducted by Millikan (1), who showed that a small current flowed through the VG, called the prebreakdown current, whose magnitude increased rapidly with increasing applied voltage until breakdown occurred. The above current was shown to be due to a process attributed to field electron emission at localized spots on the cathode surface.

EXPERIMENTAL INVESTIGATIONS

The behavior of a vacuum gap under high voltage (HV) stress depends on a large number of parameters including the type of electrode material, the shape of the electrode profile, surface preparation procedure, the gap spacing, frequency, and, most importantly, whether the VG is bridged by a solid insulator (2,3). In order to firmly establish the relationship between various independent parameters associated with the VG and its insulation capability (the breakdown strength), the test arrangement shown in Fig. 1 is commonly used.

The test gap consists of a pair of parallel plane electrodes with rounded off corners to avoid local enhancement of the applied electric field at the electrode edges. Special electrode profiles (4) are used to ascertain that the field is uniform and has a maximum value in the middle region of the VG, away from the electrode edges. The evacuation system should not introduce contaminants into the VG. Although inexpensive, fast, and rather widely used, an oil diffusion pump can contaminate the electrodes with oil due to backstreaming unless a liquid nitrogen-cooled trap is used. A turbomolecular pump backed by an oil-free diaphragm pump is a good choice to reach pressures ≤ 1 μtorr. Superior performance is obtained using ceramic HV and low voltage (LV) feedthroughs. Use of plastic parts in the test chamber degrades the final vacuum achieved due to outgassing. The HV to the test gap is derived from a low ripple regulated dc power supply provided with a vernier voltage control and an adjustable trip to shut off the power supply when the current through the VG exceeds a threshold value (e.g., 1 mA). Generally, a 100 MΩ series resistor is used to prevent excessive current flow through the VG in case of a breakdown. An electrometer (picoammeter) with a sensitivity of $\cong$0.01 pA is used in series with the test gap for prebreakdown current measurement. A series parallel combination of back-to-back fast acting diodes is necessary to protect the electrometer against accidental discharges. While a 60 kV supply is adequate for studying a 1 mm gap, a 300 kV to 400 kV supply is needed for a 1 cm gap. Precaution has to be taken for proper grounding and shielding of the test system in order to reduce background noise in the measurement system. While the testing described here uses dc voltages, many vacuum insulation requirements utilize ac, RF, or pulsed voltages.

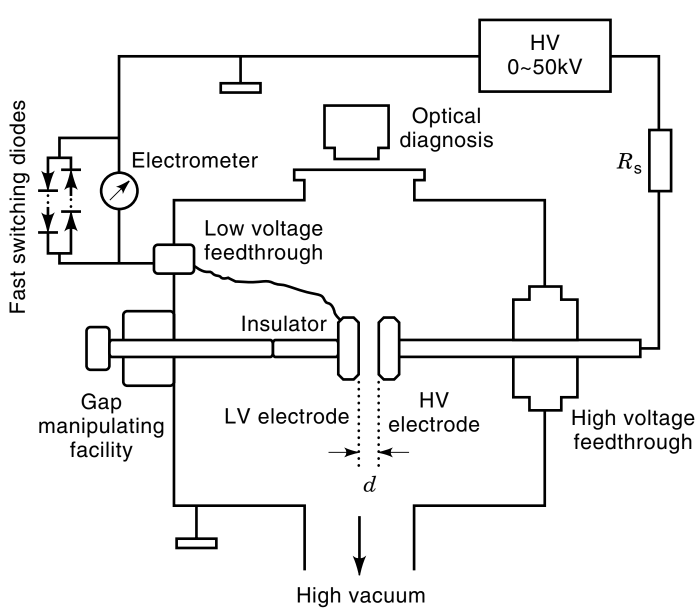

Figure 1. Schematic of the high voltage setup.

Electrode Surface Preparation

The electrodes—generally made of stainless steel, Mo, Al, or Cu (oxygen-free high purity)—are polished to a mirror finish, using successively finer grades of alumina (Al_2O_3) powder in a water slurry. The electrodes can be further subjected to chemical or electrochemical polishing prior to ultrasonic cleaning and drying. Often the electrodes are baked in situ vacuum at ~250°C to partially outgas the electrodes prior to testing. Surface contamination degrades the HV performance of a VG.

Current-Voltage (*I-V*) Characteristic

The applied voltage V is increased, waiting for a few minutes at each voltage step, until a continuous current of ≤1 pA is recorded. The voltage is then increased in smaller steps until the current I begins to increase rapidly, or becomes unstable, or unexpectedly the VG breaks down (ref. 5, Chap. 2). Figure 2 shows the typical *I-V* characteristic of a 100 μm gap between a pair of highly polished (surface roughness < 0.08 μm) chrome-steel sphere electrodes 2 cm in diameter (6). The *I-V* curve for test run no. 1 is not smooth, unlike for runs 2 and 3, a behavior attributed to electrode cleaning (conditioning), perhaps caused by gas desorption and/or modifications to electron emission sites on the cathode. The *I-V* curves in runs 2 and 3 are reproducible, indicating that the gap is conditioned. When the gap fails at the breakdown voltage V_b, an arc is produced between the anode and cathode, the gap resistance becomes very small, and the current is only limited by the external series resistance R_s.

In a broad area gap ≥5 mm, the prebreakdown current I tends to be "noisy," unlike that in Fig. 2. The average current level is superimposed with spikes known as microdischarges. The duration of these pulses varies from 50 μs to 1000 μs, with the peak current exceeding the mean value by two orders of magnitude (7,8). The microdischarges are attributable to explosive electron emission or microparticle-based subcritical events. They can also be due to ionization processes, resulting from local desorption of gas from the electrode surface (5).

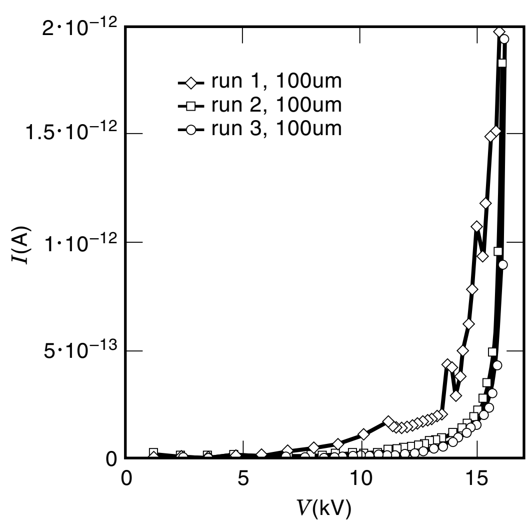

Figure 2. *I-V* curves for a 100 μm spherical gap during the first three test runs. The characteristic becomes smooth after run no. 1, indicating a conditioning effect.

In small gaps (<0.5 mm to 1 mm), a microdischarge can lead to breakdown (9), causing damage to the electrodes. As a result, in each subsequent test run, the gap holds off a lower voltage before breakdown occurs. Thus, the VG performance degrades after each breakdown. Conversely, in longer gaps (>0.5 mm), each breakdown causes an improvement (conditioning) and, after several breakdowns, the breakdown voltage is substantially higher than the first breakdown voltage (V_{b1}). For the earlier referred to 2 cm diameter spherical electrodes, for a 0.5 mm (d) gap, $V_{b1} \cong 22$ kV, while V_c, the conditioned voltage, is ≅40 kV (9). Thus for gaps ≥0.5 mm, in order to reach the full insulation capability, a VG is subjected to conditioning, a process of in situ cleaning whereby the sources of prebreakdown current and microdischarges are safely quenched so that the sources of instability that contribute to the breakdown of the gap are reduced. Since the objective is to reduce the size of the HV apparatus or device, it is important to maximize the insulation capability of a given VG. Thus, conditioning has significant practical importance, especially in long gap (>1 cm) unbaked systems, where the electrode surfaces are not extremely smooth. There are several means of conditioning the VG (5).

1. Current conditioning. Here, the voltage is increased in small steps, allowing the current to stabilize before increasing the voltage. Both the average current and the microdischarge activity decrease with time. Subsequent to the appearance of a large predischarge pulse, the mean current stabilizes to a lower value. The key to this process is the presence of a large current limiting series resistor (~100 MΩ) which reduces the voltage across the VG during the transient current spike associated with a microdischarge. If the intended insulation voltage is V_i, the step-conditioning process is continued until V_i is exceeded by a safety margin of ~25%. In an optimum gap, holdoff voltages of 10 kV and 100 kV can be achieved with gap values of 0.5 mm and 5 mm.
2. Glow discharge conditioning. Here, the pressure in the chamber is increased to ≅1 mtorr in an inert gas atmosphere (Argon) so that a low-voltage ac glow discharge is established between the electrodes (~25 mA for ~30 min). The resulting sputtering action of low energy gas ions is to remove contaminants from the electrode surfaces, thereby minimizing the microdischarge activity and increasing the threshold for the onset of breakdown. Best results are obtained by performing the glow discharge treatment in He followed by N_2 (10). After the above treatment, the chamber is re-evacuated before making the HV measurements.
3. Gas conditioning. Here, the gap is stressed to progressively higher fields in an He atmosphere (~0.1 mtorr) at currents of a few microamperes, allowing the prebreakdown current to quench over a 20 min period, until the final operating field of the gap is reached (11).
4. Spark conditioning. Here, the VG is subjected to a sequence of sparks by gradually increasing the voltage until breakdown occurs. The applied voltage is reduced to zero, or the power supply is set to automatically trip when the current in the circuit exceeds a certain value

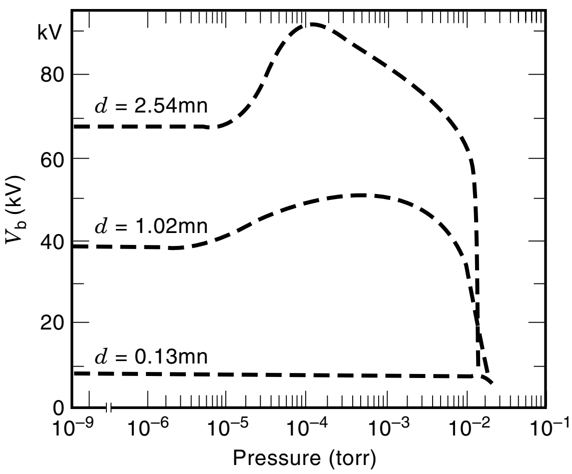

Figure 3. Variation of dc breakdown voltage versus pressure at different gap spacings, indicating the pressure effect (based on Ref. 14).

(e.g., 1 mA). The above process is repeated, typically 5 to 25 sparkings, until the gap shows no further improvement in V_b. The performance improvement is attributed to the progressive removal of selective sites on the cathode that dominate the electron emission. For this technique to be effective, the external capacitance parallel to the test gap must be minimized to limit the energy dissipated in each spike to <10 J to 20 J. It has been shown that a significant improvement in the insulation capability of a VG can be reached by subjecting it to nanosecond pulse spark conditioning (12). In fact, an electrode polishing effect is achieved by this nanosecond discharge technique.

Effect of Gas Pressure

The prebreakdown and breakdown characteristics of a VG depend strongly on the nature of the residual gas environment. The insulating properties, particularly of long gaps associated with accelerator tubes (13), also depend on the ambient pressure (14). A plot of V_b vs the pressure of dry air at different gap spacings shows a characteristic pressure p_c at which the breakdown voltage is a maximum (V_{bc}) that can be as much as 50% above the mean V_b at low pressures (<1 μtorr), as shown in Fig. 3. The values of p_c and V_{bc} depends on the electrode material, gas pressure, and the residual gas species. The pressure effect is attributed to an increase in the work function of an electron emitter following the physisorption of gas species at the higher pressure (15).

Effect of Electrode Separation

For a given electrode material and geometry, the breakdown voltage V_b is not a simple function of gap spacing d. Moreover, VGs that are apparently prepared identically exhibit significant scatter, even as high as 50%. Figure 4(a) shows V_{b1} the first breakdown voltage versus d for vacuum gaps formed between highly polished chrome-steel sphere electrodes described earlier in reference to Fig. 2. For gaps <1 mm, the electric field in the central region of the VG is nearly uniform. For gaps between 25 μm to 200 μm, V_{b1} increases steadily with gap distance according to $V_b = 37 \times d^{0.37}$ kV where d is in millimeters (9). However, for gaps 0.2 mm $< d \leq$ 1 mm, V_{b1} is weakly dependent on d, having values between 20 kV and 25 kV. However, once the gap is conditioned by spark discharges at d = 0.6 mm, for gaps 0.025 mm $< d <$ 0.6 mm, $V_b = 44.5 \times d^{0.44}$ kV (d in millimeter). The above relationships of V_b vs d are based on experimental measurements; they do not represent a fundamental law. Figure 4(b) shows the variation of the conditioned breakdown field E_b (V_b/d) versus d after the gap is fully conditioned at d = 0.6 mm (9). Thus, small gaps <0.2 mm exhibit a strong dependence of E_b on d while longer gaps >0.2 mm exhibit a much weaker dependence of E_b on d. The breakdown field decreases from ≅200 kV/mm for a 0.05 mm gap to ≅45 kV/mm for a 1 mm gap. Thus, the insulation capability per unit length decreases with increasing gap spacing. Note, for a perfect VG, the theoretical breakdown field is 6.5 MV/mm. It is believed that the small gap breakdown is dominated by an electron emission-based process, while large gap (>2 mm) behavior is dominated by microparticle exchange processes (2). The prebreakdown and breakdown characteristics of a VG strongly depend on the electrode material geometry, diameter, surface preparation, the applied voltage waveform (dc, ac, or pulse), and the external circuitry used. For a detailed study, the reader is referred to Refs. 5 and 16.

THEORETICAL CONSIDERATIONS

It has been recognized that the stable current (Fig. 2) in a VG originates from few random emission sites on the cathode

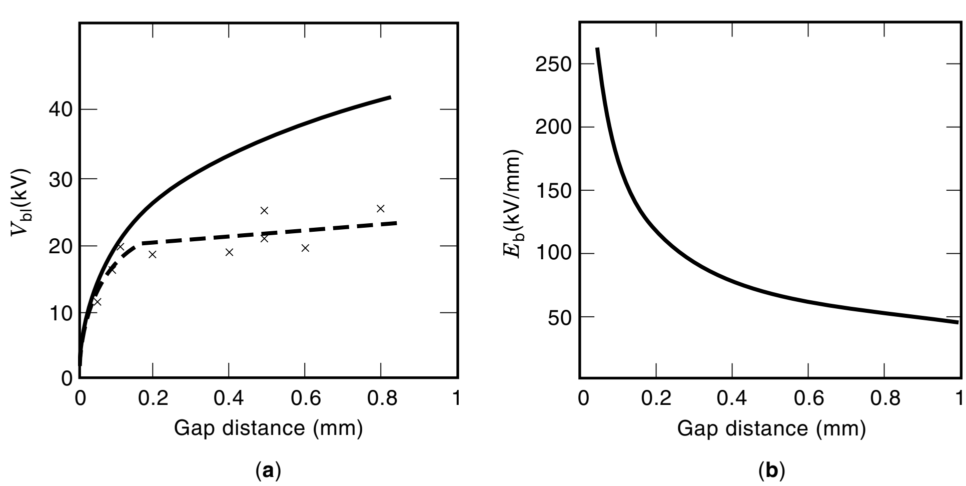

Figure 4. Dependence of vacuum gap breakdown (dc) on the electrode gap spacing. (a) Variation of "first" and "conditioned" dc breakdown voltage versus gap spacing between two highly polished spherical electrodes. The points correspond to experimental data. (b) "Conditioned" dc breakdown field versus gap spacing. Dashed curve—first breakdown, solid curve—conditioned breakdown.

(17). Millikan attributed this current to a cold-emission process, now known as a field electron emission (FEE), at localized points on the cathode (18). These emission sites were assumed to be field-enhancing microfeatures (protrusions due to the intrinsic roughness on a microscopic scale) on the cathode, where there is an effective reduction in the work function due to the Schottky effect. Using laboratory-etched microtip emitters similar to those used in a field emission microscope, Dyke (19) showed qualitatively that an electron emission obeys the well-known Fowler–Nordheim (FN) (20) quantum mechanical tunneling theory of field emission from metal surfaces. Using well-defined, point-plane electrodes, he showed that at a critical current density of ≅5 × 10^7 A/m^2, the emitting surface becomes thermally unstable, and the cathode material is vaporized, leading to breakdown initiation.

In a planar electrode system, assuming the presence of localized microprotrusions on the cathode, the microscopic field at the tip of the protrusion E_{local} is enhanced over the uniform gap field value E (V/d) by a factor β: $E_{local} = \beta E$, where β is the field enhancement factor (Ref. 5, Chap. 4). From the FN theory of electron emission, the dependence of the field emission current I on the voltage V applied to a VG is reduced to

$$I = [A_e B_1/\phi][\beta V/d]^2 \exp[-B_2 d\phi^{3/2}/\beta](1/V) \tag{1}$$

assuming that there is a single dominant emission site of area A_e.

$$\ln(I/V^2) = k_1 - k_2(1/V) \tag{2}$$

where

$$k_1 = \ln[(A_e B_1/\phi)(\beta^2/d^2)]$$

and

$$k_2 = -B_2 d\phi^{3/2}/\beta$$

$$B_1 = 1.54 \times 10^{-6} \text{ and } B_2 = 6.83 \times 10^9$$

Thus, if the FN type of electron emission is responsible for the prebreakdown emission current, a plot of in(I/V^2) versus $1/V$ should produce a straight line, which has been confirmed for a wide range of fields. In Eq. (2), assuming the work function of the material ϕ (≅4.5 eV for most electrode materials), from the slope of the straight line k_2 we can obtain β, and the effective emitting area A_e can be found from the intercept k_1. Typical values reported are $100 \leq \beta \leq 1000$ and $10^{-16} \leq A_e \leq 10^{-12}$ m^2.

For the sphere electrode gap discussed earlier (Fig. 4), conditioned at $d = 0.6$ mm, the FN plots at different gap spacings are shown in Fig. 5. Note that the straight line approximation is good for gaps $d > 0.5$ mm (6).

In contrast to the classical metallic microprotrusion model, recent work by Latham indicates that the emission is due to various contaminating microstructures (metal-insulator-metal and metal-insulator-vacuum), called electron pin-holes, that are found on typical HV electrodes (21). Electrons can flow out of these microfeatures at fields that are two or three orders of magnitude below the theoretical threshold value of 3 × 10^9 V/m required for the microprotrusion emission mechanism.

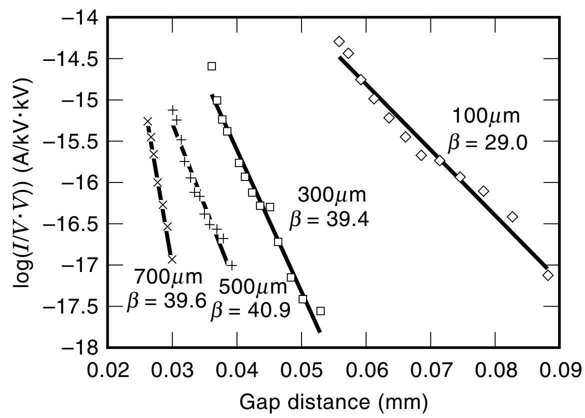

Figure 5. Fowler–Nordheim plot at different gap spacings for spherical electrodes. The β values are also indicated.

SURFACE FLASHOVER

Solid insulator spacers bridging a VG degrades the insulation performance. A solid insulator is inevitable in any HV vacuum system, either for mechanical support (spacer) or for electrical insulation of the HV electrode from ground. Failure occurs by a discharge propagating along the insulator/vacuum interface between the two electrodes by a process called surface flashover. The solid insulator is the weakest link electrically. For a 5 mm VG formed between a pair of unbaked parallel plane electrodes 10 cm in diameter, $V_b \cong 120$ kV dc while bridging the above gap with an alumina insulator 14 mm diameter causes flashover at ≅ 40 kV.

The breakdown strength of an insulator-bridged gap decreases with increasing gap spacing. In a parallel plane electrode system, under identical conditions, for Al_2O_3 ceramic insulators 14 mm in diameter, $E_b \cong V_b/d = 12$ kV/mm for $d = 2$ mm; 8 kV/mm for $d = 5$ mm; 5.3 kV/mm for $d = 10$ mm; 5.1 kV/mm for $d = 12.7$ mm (22). These are examples of reported measurements; the values very much depend on material parameters and experimental conditions. Coating the insulator surface with low secondary emission yield materials significantly improves E_b. For alumina coated with Cr_2O_3, $E_b = 13.5$ kV/mm, a significant improvement from 5.1 kV/mm for an uncoated sample $d = 12.7$ mm. Such coatings reduce the charging of the insulator surface. Likewise, increasing the surface conductivity somewhat by doping alumina with Mn–Ti resulted in improvements of 30% to 40% in V_b (23).

Simple modifications to the insulator shape has a significant influence on the flashover strength of insulators. For example, incorporating a 55° angle bevel near the cathode end of a cylindrical insulator improves V_b to >100 kV, compared to 45 kV for a straight unbeveled PMMA insulator $d = 9$ mm long and 4.84 cm diameter (24). Likewise for the above 9 mm long PMMA spacer, V_b increases from 45 kV to >100 kV by changing the shape to a conical frustrum whose base is in contact with the anode at an angle $\theta = 50°$. For microsecond-long pulse excitations, the breakdown strength of a 45° conical frustrum (cone base at the cathode) is about three times larger than that of a straight cylinder (25).

Insulator-bridged gaps also exhibit conditioning with V_b increasing after each successive flashover until a maximum is reached. Degradation of the insulator, resulting in tracking, occurs if the insulator is subjected to additional flashovers, called deconditioning. The degree of conditioning (above the first V_b) can vary from 10% to 100%, depending on the conditions of the gap.

Extensive studies have been done on the role of insulator material, impurity content, size, shape, surface microstructural properties such as grain boundary defects, porosity, surface damage caused by mechanical abrasion, and the design of the interface between the metal-insulator-vacuum, called the triple junction (Ref. 5, Chap. 28; Ref. 26). Several physical models are proposed to describe the flashover process; they are based on either some kind of a charge cascading process along the solid/vacuum interface or charge localization on the surface leading to the buildup of the local field to a point of instigating a breakdown (24,26,27).

APPLICATIONS

In general, vacuum breakdown is a threat to electrical insulation of a system in many vacuum applications, yet a vacuum discharge can be put to use, as in vacuum circuit breakers used in power delivery or ion beam arcs used for high adhesion, hard, and corrosion-resistant coatings (28). Pulsed power systems draw energy from a source at low voltage and power and deliver large peak powers (at high voltages) to loads that generate EM radiation or particle beams as, for example, microwave, RF, laser, X-rays, pulsed radar, kinetic energy weapons, or a high energy particle beam for fusion or the simulation of nuclear-generated electromagnetic pulses (29). Generally, vacuum breakdown problems arise at such loads. Vacuum insulation and discharges are key issues in triggered vacuum switches used as closing and opening switches in pulse power systems.

In the commercial arena, vacuum insulation and breakdown issues are critical in such devices as electron beam guns, X-ray generators, and microwave tubes (TWTs and klystrons). In the exotic arena of pulsed power, applications include the treatment of flue gases, food preservation and processing, metal forming, toxic waste processing, and particle- and photon-based radiation therapies. For the fabrication of next-generation microchips that are even smaller and faster, lithography based on pulsed X-rays is needed (5).

Modern electron and proton accelerators use superconducting cavities (niobium) for high energy physics research and drivers for free electron lasers. The need to achieve higher accelerating gradients requires deeper understanding of electron emission from surfaces that can trigger a vacuum breakdown (30).

There are key vacuum insulation and breakdown issues related to space power systems and space vehicles and platforms with a potential for savings in spacecraft mass and cost (5). The voltage level of an exposed spacecraft power-bus system is determined by the properties of the space vacuum. The environment in space is conducive to spacecraft charging and subsequent breakdown.

BIBLIOGRAPHY

1. R. A. Millikan and R. A. Sawyer, Extreme ultraviolet spectra of hot sparks in high vacua, *Phys. Rev.,* **12**: 167–170, 1918.
2. R. Hawley and A. Maitland, *Vacuum as an Insulator,* London: Chapman and Hall, 1967.
3. R. Hawley, Solid insulators in vacuum: A review, *Vacuum,* **18**: 383–390, 1968.
4. J. A. Harrison, A computer study of uniform-field electrodes, *Br. J. Appl. Phys.,* **18**: 1617–1622, 1967.
5. R. Latham, *High Voltage Vacuum Insulation,* London: Academic Press, 1995.
6. X. Ma and T. S. Sudarshan, Prebreakdown and breakdown characteristics of micrometric vacuum gaps between broad area electrodes, *Conf. Electr. Insul. Dielect. Phenomena,* Minneapolis, MN, 1997.
7. H. Boersch, H. Hamisch, and S. Wiesner, Electrical microdischarges in vacuum, *Z. Agnew. Phys.,* **13**: 450–456, 1961.
8. H. P. S. Powell and P. A. Chatterton, Prebreakdown conduction between vacuum insulated electrodes, *Vacuum,* **20**: 419–429, 1970.
9. X. Ma and T. S. Sudarshan, High field breakdown characteristics in micrometric gaps in vacuum, *10th Int. Vac. Microelectron. Conf.,* Kyongju, Korea, 1997.
10. R. Hackam and G. Govinda Raju, Electrical breakdown in a point-plane gap in high vacuum and with variation of pressure in the range 10^{-7} -10^{-2} Torr of air, nitrogen, helium, sulphur hexafluoride and argon, *J. Appl. Phys.,* **45**: 4784–4794, 1974.
11. G. P. Beukema, Conditioning of a vacuum gap by sparks and ion bombardment, *Physica C,* **61**: 259–274, 1972.
12. B. Juttner, On the polishing effect of nanosecond discharges in vacuum, *Beitr. Plasmaphys.,* **19**: 259–265, 1979.
13. J. L. McKibben and K. Boyer, Current loading in ion accelerating tubes, *Phys. Rev.,* **82**: 315–316, 1951.
14. R. Hackam and L. Altcheh, AC (50 Hz) and DC electrical breakdown of vacuum gaps and with variation of air pressure in the range 10^{-9} -10^{-12} Torr using OFHC copper, nickel, aluminum, and niobium parallel planar electrodes, *J. Appl. Phys.,* **46**: 627–636, 1975.
15. B. Juttner, H. Wolff, and B. Altrichter, Stability of field electron emission and vacuum breakdown. Investigations with field emission microscopy and auger electron spectroscopy, *Phys. Status Solidi.,* **A27**: 403–412, 1975.
16. R. J. Noer, Electron field emission from broad-area electrodes, *Appl. Phys. A,* **A28**: 1–24, 1982.
17. G. A. Farrall, Correlation of electrical breakdown and centers of strong electron emission on a zone-refined iron cathode in vacuum, *J. Appl. Phys.,* **42**: 2284–2293, 1971.
18. R. A. Millikan and B. E. Shackelford, On the possibility of pulling electrons from metals by powerful electric fields, *Phys. Rev.,* **15**: 239–240, 1920.
19. W. P. Dyke and J. K. Trolan, Field emission: Large current densities, space charge, and the vacuum arc, *Phys. Rev.,* **89**: 799–808, 1953.
20. R. H. Fowler and L. Nordheim, Electron emission in intense electric fields, *Proc. R. Soc. London,* **A119**: 173–181, 1928.
21. N. K. Allen and R. V. Latham, The energy spectra of high-electron emission sites on broad-area copper electrodes, *J. Phys. D,* **11**: L55–L57, 1978.
22. N. C. Jaitly and T. S. Sudarshan, X-ray emission and prebreakdown currents in plain and dielectric bridged vacuum gaps under DC excitation, *IEEE Trans. Electr. Insul.,* **23**: 231–242, 1988.
23. N. C. Jaitly et al., Degradation due to wet hydrogen firing on the high voltage performance of alumina insulators in vacuum applications, *IEEE Trans. Electr. Insul.,* **22**: 447–452, 1987.
24. N. C. Jaitly and T. S. Sudarshan, DC surface flashover mechanism along solids in vacuum, based on a collision ionization model, *J. Appl. Phys.,* **67**: 3411–3418, 1988.

25. O. Milton, Pulsed flashover of insulators in vacuum, *IEEE Trans. Electr. Insul.,* **EI-7**: 9–15, 1972.
26. H. C. Miller, Surface flashover of insulators, *IEEE Trans. Electr. Insul.,* **24**: 765–786, 1989.
27. G. Blaise, Space-charge physics and breakdown process, *J. Appl. Phys.,* **77** (7): 2916–2927, 1995.
28. R. L. Boxman, P. J. Martin, and D. M. Sanders, *Handbook of Vacuum Arc Science and Technology,* Park Ridge, NJ: Noyes Publications, 1995.
29. T. H. Martin, A. H. Guenther, and M. Kristiansen (eds.), *J. C. Martin on Pulsed Power,* New York: Plenum, 1997.
30. P. Kneisel, Radio-frequency superconductivity technology: Its sensitivity to surface conditions, *J. Vac. Sci. Technol.,* **A11**: 1575–1583, 1993.

TANGALI S. SUDARSHAN
University of South Carolina